PCT WORLD INTELLECTUAL PROPERTY ORGANIZATION
International Bureau

INTERNATIONAL APPLICATION PUBLISHED UNDER THE PATENT COOPERATION TREATY (PCT)

(51) International Patent Classification 6 : H01L 33/00, H01S 3/085

A1

(11) International Publication Number: WO 98/25313

(43) International Publication Date: 11 June 1998 (11.06.98)

(21) International Application Number: PCT/GB97/03356

(22) International Filing Date: 4 December 1997 (04.12.97)

(30) Priority Data:
9625332.3 5 December 1996 (05.12.96) GB

(71) Applicant *(for all designated States except US)*: BRITISH TECHNOLOGY GROUP LIMITED [GB/GB]; 10 Fleet Place, London EC4M 7SB (GB).

(72) Inventors; and

(75) Inventors/Applicants *(for US only)*: BARNES, William, Leslie [GB/GB]; 49 Retreat Road, Topsham, Exeter EX3 0LF (GB). KITSON, Stephen, Christopher [GB/GB]; Osprey Lodge, 1 Avenue Road, Malvern, Worcester WR14 3AG (GB). SAMBLES, John, Roy [GB/GB]; Shirley House, Copplestone, Crediton EX17 5NS (GB).

(74) Agent: CULLIS, Roger; British Technology Group Limited, Patents Dept., 10 Fleet Place, London EC4M 7SB (GB).

(81) Designated States: JP, US, European patent (AT, BE, CH, DE, DK, ES, FI, FR, GB, GR, IE, IT, LU, MC, NL, PT, SE).

Published
With international search report.

(54) Title: RADIATION EMITTING DEVICES

(57) Abstract

A radiation emitting device includes an optical micro–cavity bounded by first and second reflective boundaries (33, 39), at least one of said reflective boundaries (39) has associated therewith inhibiting means, such as an array of hillocks or dimples, to inhibit the coupling of radiation from within the micro–cavity (31) to predetermined propagation modes, such as surface plasmon polaritons, associated with at least one of the reflective boundaries.

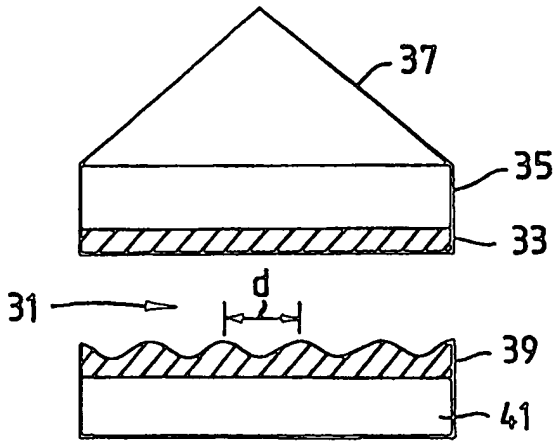

FOR THE PURPOSES OF INFORMATION ONLY

Codes used to identify States party to the PCT on the front pages of pamphlets publishing international applications under the PCT.

AL	Albania	**ES**	Spain	**LS**	Lesotho	**SI**	Slovenia
AM	Armenia	**FI**	Finland	**LT**	Lithuania	**SK**	Slovakia
AT	Austria	**FR**	France	**LU**	Luxembourg	**SN**	Senegal
AU	Australia	**GA**	Gabon	**LV**	Latvia	**SZ**	Swaziland
AZ	Azerbaijan	**GB**	United Kingdom	**MC**	Monaco	**TD**	Chad
BA	Bosnia and Herzegovina	**GE**	Georgia	**MD**	Republic of Moldova	**TG**	Togo
BB	Barbados	**GH**	Ghana	**MG**	Madagascar	**TJ**	Tajikistan
BE	Belgium	**GN**	Guinea	**MK**	The former Yugoslav Republic of Macedonia	**TM**	Turkmenistan
BF	Burkina Faso	**GR**	Greece			**TR**	Turkey
BG	Bulgaria	**HU**	Hungary	**ML**	Mali	**TT**	Trinidad and Tobago
BJ	Benin	**IE**	Ireland	**MN**	Mongolia	**UA**	Ukraine
BR	Brazil	**IL**	Israel	**MR**	Mauritania	**UG**	Uganda
BY	Belarus	**IS**	Iceland	**MW**	Malawi	**US**	United States of America
CA	Canada	**IT**	Italy	**MX**	Mexico	**UZ**	Uzbekistan
CF	Central African Republic	**JP**	Japan	**NE**	Niger	**VN**	Viet Nam
CG	Congo	**KE**	Kenya	**NL**	Netherlands	**YU**	Yugoslavia
CH	Switzerland	**KG**	Kyrgyzstan	**NO**	Norway	**ZW**	Zimbabwe
CI	Côte d'Ivoire	**KP**	Democratic People's Republic of Korea	**NZ**	New Zealand		
CM	Cameroon			**PL**	Poland		
CN	China	**KR**	Republic of Korea	**PT**	Portugal		
CU	Cuba	**KZ**	Kazakstan	**RO**	Romania		
CZ	Czech Republic	**LC**	Saint Lucia	**RU**	Russian Federation		
DE	Germany	**LI**	Liechtenstein	**SD**	Sudan		
DK	Denmark	**LK**	Sri Lanka	**SE**	Sweden		
EE	Estonia	**LR**	Liberia	**SG**	Singapore		

Radiation emitting devices

This invention relates to radiation emitting devices and, in particular, to an improved manner of construction for light emitting diodes. More particularly, but not exclusively, the invention relates to a micro-cavity for use in light emitting diodes.

Light emitting diodes (LEDs) comprise a light (radiation) emitting substance usually in the form of a thin film. This light emitting substance is usually positioned inside a mirrored cavity, sometimes called a micro-cavity. Two mirrors are used to form the micro-cavity and one of the mirrors is more reflective than the other. The less reflective of the two mirrors permits radiation to pass through it and escape from the micro-cavity, thus providing useful output light from the device.

Generally, the efficiency of an LED is increased by improving coupling between radiation modes of the micro-cavity and the light emitting substance. One way of achieving this is to ensure that the separation between the mirrors is of the order of the wavelength of the desired output radiation.

There are two types of mirror which have been used in LEDs. These are the distributed Bragg reflector (DBR) – usually made from alternating layers of different refractive index materials – and metallic mirrors. DBRs may be highly reflective, but only over a relatively narrow range of incident angles. Light incident at other angles leaks from the micro-cavity in the form of wasted output. Metallic mirrors however are reflective over a wider range of incident angles, but have losses associated with the absorption of the metal. Because metallic mirrors are generally thinner than the wavelength of light they allow the fabrication of very compact devices.

When light emitters, envisaged as point sources (and assumed to be oscillating electric dipoles), are near the surface of a metallic mirror they may couple to the so-called surface plasmon polariton (SPP) mode of that surface. This coupling is strongest when the separation between the emitter and mirror is approximately 1/60 of the order of the wavelength of the desired output radiation. However, coupling is still significant at approximately ½ of the wavelength of the desired output radiation. The coupling arises despite the surface plasmon polaritons (SPPs) being non-radiative, due to the non-planar nature of the dipole field of the emitter in the near field regime.

High momentum components of the near field part of the dipole field can couple to the SPP mode without the need for further momentum matching. These near field components in the dipole field are sometimes known as evanescent waves. The result is that, for a typical micro-cavity operating in the visible region of the electromagnetic radiation (EMR) spectrum close to the lowest order mode cut-off of the micro-cavity, approximately 50% of the energy is wasted in generating SPPs rather than in producing useful, emitted radiation.

Loss of energy to SPP coupling and losses in metal layers represent wasted output. This problem has been discussed in publications in *Physical Review A*, **51**, pp 4116-4122, 1995 by Abram and Oudar, and in *Optics Communications*, **100**, pp 259-267, 1993 by Tomas and Lenac. These authors discuss the use of metallic mirrors in micro-cavities, the problems associated with loss due to the metals and the implications of this loss for light emitting diodes (LEDs).

The inventors have realised that in order to improve the quantum efficiency of an LED it is desirable to remove the unwanted coupling between the emitters and the SPP modes. This applies particularly to micro-cavities formed from two metallic mirrors and those formed from one metallic mirror and one DBR mirror. Since the primary reason for the wasted energy is the generation of surface plasmon polaritons, removing this mode from the micro-cavity is required in order that the efficiency can be improved.

It is therefore an aim of the present invention to provide an improved micro-cavity suitable for use in a more efficient light emitting device (for example light emitting diode (LED)), the device having a higher quantum efficiency of conversion of internal energy to useful radiated energy.

According to the present invention there is provided a radiation emitting device including an optical micro-cavity bounded by first and second reflective boundaries wherein at least one of said reflective boundaries has associated therewith inhibiting means to inhibit the coupling of radiation from within the micro-cavity to predetermined propagation modes associated with at least one of said first and second reflective boundaries.

There is also provided a radiation emitting device including an optical micro-cavity comprising first and second mirrors in which at least one of said mirrors has a substantially non-planar surface.

According to a further aspect of the present invention there is provided a light emitting device (e.g. LED) comprising first and second mirrors, one or both of which are metallic, defining a micro-cavity and a light emitting substance disposed in the micro-cavity, wherein at least one of the mirrors has a substantially non-planar surface.

According to another aspect of the present invention there is provided a light emitting device comprising a light emitting substance interposed between a first and a second mirror, each mirror having a surface, the mirrors defining a micro-cavity, wherein means is provided for establishing a photonic band gap substantially to reduce the coupling of energy from within the micro-cavity, to modes associated with at least one mirror surface.

According to a further aspect of the present invention there is provided a method of fabricating a radiation emitting device including a substrate with a repeating pattern comprising the steps of causing a master pattern to induce a first repeating pattern to be formed on the substrate, rotating the master pattern with respect to the substrate and inducing a second repeating pattern to be formed on the substrate, the two repeating patterns sharing a common region.

The non-planar mirror(s) or reflector(s) may be fabricated according to the method hereinafter described and is/are preferably in the form of an array of "hillocks" or "dimples", having a repeating pattern. The pattern may be generally rectangular, but is preferably, generally hexagonal.

Portions of substrate may be selectively removed by etching techniques such as ion beam lithography, photo-lithography or chemical etching.

According to yet a further aspect of the present invention there is provided a method of manufacturing a radiation emitting device incorporating a sub-micron, repeating pattern in or on a dielectric substrate comprising the steps of placing a pattern bearing mask between the surface of the substrate and an energy source, exposing the substrate to the energy source and forming a pattern rotating the mask with respect to the substrate, re-exposing the surface of the substrate to the energy source thereby

forming another pattern and selectively removing portions of exposed or non-exposed substrate, so as to reveal a repeating pattern on or in the substrate.

Preferably the pattern is in the form of a plurality of regularly spaced, undulating regions. Advantageously these regions are in the form of raised circularly symmetric "hillocks" or "dimples" and the overall effect of such a surface approximates closely to a circular Brillouin zone.

Preferably the substrate is fabricated by using a system of multiple exposures in a standard two beam interferometer. Preferably three exposures, with the substrate rotated by 60° between each exposure, is required in to obtain an hexagonal structure. However, this requires a high degree of precision by ensuring all three exposures are exactly in register. In practice this is difficult. Most preferably two exposures may be made, followed by selective partial etching in order to achieve a desirable intensity profile of pattern across the substrate.

The invention will now be particularly described by way of example with reference to the accompanying drawings, in which:–

Figure 1 shows a theoretical prediction in the form of a logarithmic scaled graph of the energy dissipated due to different causes, as a fraction of the total energy available for the production of radiation from an LED with metallic mirrors.

Figure 2 shows a dispersion curve for a micro-cavity with metallic mirrors.

Figure 3 is a schematic view of a micro-cavity used to demonstrate the prohibition of the SPP decay channel;

Figure 4 is a graph of the measured dispersion curve for the micro-cavity depicted in Figure 3.

Figure 5 is a schematic diagram of one possible LED structure that exhibits improved efficiency by incorporating a non-planar mirror for one of the mirrors that forms the micro-cavity;

Figure 6 is a scanning electron micrograph (SEM) image of a non-planar metallic surface that exhibits photonic band gap for surface plasmon polariton modes in the red part of the visible spectrum.

Figure 7 is a theoretically produced intensity distribution for the exposure of photoresist to two grating patterns, oriented at 60 degrees with respect to each other;

Figure 8 is a schematic of the prism coupling technique used to measure the SPP band gap (i.e. band structure) of a textured surface similar to that shown in Figure 5;

Figure 9 is the measured dispersion curve for surface plasmon polarity modes propagating on a surface similar to the one shown in Figure 6.

Figure 10 shows how the energy of the band gap edges. Figure 9, vary with propagation angle.

Referring to the drawings, a graphical illustration of the relative importance of different decay channels is shown below in Figure 1, which depicts (on a logarithmic scale) relative amounts of energy, generated in a micro-cavity. The integrals under the different regions of the curve indicate the relative values of energy dissipated. Region 1 represents energy dissipated as potentially useful radiation. Region 2 represents energy dissipated coupling to SPP modes on all metal surfaces of mirrors. Region 3 represents energy losses due to the metal and are important only for emitters very close (i.e. less than approximately 1/60 the wavelength of the radiation) to the metal. It is apparent that the area in region 1, which is potentially useful radiation, represents approximately 50% of the total theoretical energy available.

For small values of micro-cavity (d) (where d is the inter-mirror spacing and is less than approximately 20nm), the lifetime of a light emitting device rapidly drops as fluorescence is quenched.

Blocking the propagation of modes in all directions requires a repeating pattern with a Brillouin zone that is as close to circular as possible. A surface with hexagonal symmetry is a reasonable approximation to this pattern.

The desired effect of a non-planar mirror on the surface plasmon polariton modes. i.e. prohibiting their propagation. is demonstrated with a simple micro-cavity structure as described below with reference to Figure 3. The allowed modes of the metallic mirrored micro-cavity are represented on a dispersion curve, in Figure 2. The frequency of allowed modes, as a function of in-plane wave vector, k_x is shown. The

dipole emitters have a fixed frequency, but may couple to modes with any value of k_x at that frequency. The desired radiation mode of the micro-cavity is also indicated on Figure 2 as feature 1. It is seen from Figure 2 that another mode, indicated as feature 2 in Figure 2, is also present at the same frequency as feature 1. Feature 2 is a surface plasmon polariton (SPP) mode of the metallic micro-cavity. By corrugating one of the metallic surfaces this unwanted mode can be eliminated. Figure 3 shows a cavity 31 between a planar silver layer 33 on a glass plate 35 provided with a glass prism 37 and a corrugated optically-thick silver layer 39 on a glass substrate 41. This is a schematic view of a micro-cavity used to demonstrate the prohibition of the SPP decay channel.

Corrugation is preferably in the form of a repeating ('periodic') pattern. Preferably the pattern required is in the form of a non-planar surface and comprises an array of "hillocks" or "dimples" arranged so that the distance between "hillocks" or "dimples", d, is given approximately by,

$$2k_{spp} = 2\pi/d$$

(where k_{spp} is the wave vector of a surface plasmon polariton).

The non-planar surface of one of the mirrors (or reflectors) effectively generates a broad photonic band gap for surface plasmon polaritons (SPPs) and thereby reduces the overall loss of energy from the light emitting device which has hitherto occurred due to coupling between the light emitters and the SPP modes of the metallic mirrors. The radiation efficiency of the device is thus greatly improved.

An optical or electrical pump source may be fabricated integrally with the light emitting device or it may added as a part finished device for subsequent use.

Surface plasmon polaritons are non-radiative TM polarised modes that propagate at the interface between a metal and a dielectric. The inventors have realised that in order to generate a photonic band gap, a wavelength scale periodicity has to be introduced. For a surface plasmon polariton this may be readily achieved by corrugating the metal/dielectric surface of a mirror defining the micro-cavity. However, it will be appreciated that other ways of achieving this objective may be possible, including for example and without limitation, modulating the or each refractive index of the material(s) within the micro-cavity.

A corrugated surface however, only blocks the propagation of surface plasmon polaritons over a narrow range of directions. In order to generate a full band gap, (that is one that will block the propagation of surface plasmon polaritons in all directions on the surface), a more complex periodic structure is required. This is necessary if blocking the propagation of surface plasmon polaritons is to have a significant effect on the properties of metallic micro-cavities.

A theoretical prediction in the form of a logarithmic scaled graph of the energy dissipated, due to different causes, as a fraction of the total energy available for the production of radiation from an LED with metallic mirrors is shown in Figure 1. The dipole moments that make up the emitters are assumed to be randomly oriented and dispersed throughout the region between the mirrors;

Figure 2 shows the dispersion curve for a micro-cavity with metallic mirrors. TE is the lowest order transverse electric mode of the micro-cavity, TM is normally the lowest order transverse magnetic mode of a micro-cavity, but, because the mirrors of the micro-cavity depicted are metallic, another mode exists, namely the surface plasmon polariton mode, (SPP). A light emitting diode based on a micro-cavity may be operated on or around cut-off, i.e. at a frequency marked as f_c. The presence of the SPP mode at this frequency provides an unwanted loss mechanism for the dipole emitters located within the micro-cavity.

Figure 4 is a graph of the measured dispersion curve for the micro-cavity depicted in Figure 3. Feature 1 is the lowest order radiative mode, namely the one into which it is desired the emitters couple to produce a useful output from the device. The unwanted surface plasmon polariton mode is depicted as being blocked by a band gap, (feature 2); contrast this with the dispersion curve of the planar cavity, Figure 3. By adjusting the pitch of the corrugation this gap can be made to coincide with the frequency of the lowest order radiative mode, feature 1 of Figure 4, thus preventing or eliminating loss due to coupling between emitters and surface plasmon polariton modes. This prevents or eliminates loss due to coupling between emitters and surface plasmon polariton modes. This band gap pertains to only one direction of SPP mode propagation. An array of "hillocks" or "dimples" produces a band gap in all

propagation directions (as described below) and thus eliminates or prevents the wasteful SPP coupling in light emitting devices in all directions.

Figure 5 is a schematic diagram of one possible light emitting diode structure that exhibits improved efficiency by incorporating a non-planar mirror for one of the mirrors that forms the micro-cavity. It has a substrate 51 which carries a textured lower metal mirror 53. An optical cavity 55 includes a light emitting substance. Useful optical radiation is emitted through a thin top mirror 59.

Figure 6 is a scanning electron micrograph of such a surface with a periodicity suitable for work at optical frequencies. The "hillocks" or "dimples" are formed from a photoresist deposited onto a fused silica substrate. The whole surface is subsequently coated with a relatively thick silver film which is preferably in the region of 20-60nm and most preferably substantially more than 40nm thick. The silver film supports the propagation of surface plasmon polaritons. The fabrication and operation of this structure is described in greater detail below.

Figure 7 shows an intensity map which does not have full hexagonal symmetry. This pattern is achieved by exposing the substrate only twice. There is, however, an hexagonal array of dark regions 71 that have received relatively low amounts of exposure. By making use of the fact that there is a threshold value of exposure needed to affect photoresist, it is possible to remove all the exposed parts of the substrate, leaving just the aforementioned unexposed regions. This technique subtly achieves the same effect as three exposures and only requires two exposures, whilst still revealing an hexagonal array of "hillocks" or "dimples". The advantage is that only two exposures are required and these are achieved with relative rotation of mask and substrate. The resultant effect is easier to attain because it is easier to expose a repeating linear pattern, rotate the pattern (with respect to the substrate) and re-expose the same pattern: than to try and ensure co-registration of three repeating linear patterns on a sub-microscopic scale.

In order to measure optically the band structure of surface plasmon polaritons (SPPs) a method is needed to couple the SPPs to photons. The surface modes are non-radiative, so that at a given energy SPPs have a larger wave vector than a photon of the same frequency. In order to provide coupling, the wave vector of the photon has to be

enhanced. This can be done using a standard prism coupling technique as shown for example in Figure 8. The uncoated face 81 of a fused silica substrate is brought into contact with a silica prism 83, by means of a matching fluid (not shown). Monochromatic radiation k_0, incident through the prism, may then excite surface plasmon polaritons which propagate on the air/silver interface. Energy is absorbed from the beam, reducing the reflectivity. For a given photon energy, resonant coupling occurs when the in-plane component of the photon wave vector (k_x) matches the surface plasmon wave vector (k_{spp}). That is when θ satisfies the relation

$$nk_0 \sin\theta = k_{spp}$$

where n is the refractive index of the prism and k_0 is the vacuum wave vector of the incident photon.

The band structure was measured by recording reflected intensity as a function of the photon energy and k_x. A white light source and a computer controlled spectrometer were used to produce a collimated TM polarised monochromatic beam in the wavelength range 400nm to 800nm. The angle of incidence was controlled by placing the sample on a computer controlled rotation stage capable of 0.01° resolution.

Figure 9 shows a typical set of reflectively data recorded in this way. The regions of low reflectivity (dark) are a result of photons that have been absorbed through the resonant excitation of surface plasmons. Since these photons match both the energy and the wave vector of the surface plasmon polaritons, the dark bands in Figure 9. directly map out the dispersion curve of the surface mode. There is a clear gap in the dispersion curve centred around 1.98eV. The reflectivity data is expressed as photon energy (eV) as a function of k_x. Lighter regions represent high reflectivity and darker regions correspond to low reflectivity. The dark triangle (Q) in the lower right corner is an artefact of the measurement technique. The propagation direction ψ is defined with respect to one of the principal Bragg vectors. Experimentally this may be determined by diffracting a 457.9nm wavelength beam from an argon ion laser.

In order to map out the entire band structure of the surface plasmon. dispersion curves were recorded for the full range of propagation directions. Surface plasmons excited via the aforementioned prism coupling propagate in the direction defined by the plane of incidence of the photons. The propagation direction is determined therefore by

the angle between the plane of incidence and a particular Bragg vector in the textured surface as seen in Figure 10.

The dispersion curve for each direction exhibits a clear gap, the energies of the upper and lower branches depending on ψ is shown in, Figure 10. It is clear that there is a full gap between 1.91eV and 2.00eV. That is there are no propagating modes in this energy range in any direction on the silver/air interface.

An example of one method of fabricating a substrate having a repeating sub-micron hexagonal array is described in detail in *IEEE Photonics Technology Letters* 8 No. 11.

An hexagonal array is made by first exposing the substrate twice to the same interference pattern, with the substrate rotated by 60° about its surface normal between exposures. For each exposure, the intensity profile in the interference pattern is sinusoidal. Figure 7 shows the sum of two such interference patterns and represents the total exposure at each point across the photoresist film. This pattern does not have hexagonal symmetry. In principle, hexagonal symmetry could be achieved by making a third exposure with the substrate rotated by a further 60° , but this would require setting the interference pattern exactly in register with the previous two. As this would mean aligning the sample accurately on a sub-micron scale, this is not generally practicable.

An alternative approach is to make use of nonlinearities in the fabrication process to generate additional Fourier components in the surface topography of the substrate. In particular, the aim is to produce a strong component that is the sum of the two components present in the double exposure. True hexagonal symmetry requires that these three components have the same magnitude. The nonlinearities arise from the solubility response of the photoresist to exposure and the finite thickness of the film.

The solubility response of photoresist as a function of exposure exhibits a threshold value below which the solubility is relatively unaffected, and a saturation level at very high exposures. A positive photoresist was used so that the regions exposed to less than the threshold value remain insoluble in the developer. In Figure 7 there is an hexagonal array of points (dark) which receive a very low exposure. It is these points that form the "hillocks" or "dimples" in the final structure. By controlling the exposure level, it is possible to ensure that all other regions of the film receive an above-threshold

exposure and so will be soluble to some extent. Upon development, these regions begin to dissolve and become thinner, producing a surface texture that reflects the exposure pattern (Figure 7). However, because the film is thin (typically 0.5 μm), the exposed regions will eventually completely dissolve to leave an hexagonal array of photoresist "hillocks" or "dimples" 71 on the substrate surface (Figure 7). This model predicts that the surface cannot have true hexagonal symmetry: the "hillocks" or "dimples" in Figure 6 are not circular in cross section but are elongated in one direction. This feature however was not observed experimentally (Figure 6). It may be that the development process acts to round off the "hillocks" or "dimples".

Figure 6 is an SEM of a structure fabricated with a positive resist. Shipley S1805 photoresist was used, mixed 1:1 with Hoechst AZ thinners. The photoresist was spin-coated at 4000 rpm onto an optically flat glass substrate and baked at 95°C for 30 min to remove residual solvent. The film was exposed twice in the interferometer, the substrate being rotated by 60° between exposures. In each case, the film was exposed to around 3 Jcm^{-2} of 457.9nm wavelength radiation from an argon ion laser. The photoresist was subsequently developed for 4.5 min in a solution of Microposit™ developer diluted 1:1 with deionised water. It was found that control of the developer concentration was critical. If the developer was too concentrated then it removed all the photoresist. If it was too dilute then it failed to dissolve the film fully even in the most exposed regions.

The structure in Figure 6 is not truly hexagonal because of inaccuracies in setting the rotation angle of 60°. Figure 6 includes a schematic diagram showing the dimensions of the array, determined by measuring the diffraction of 457.9nm light. The uniformity of the array is very good with few defects and with "hillocks" or "dimples" of very similar sizes, around 100nm radius.

The periodicity of the array is readily controlled by the angle of incidence θ of the two beams in the interferometer. The radius of the "hillocks" or "dimples" depend on the periodicity of the interference pattern, the value of the threshold exposure, and on the total exposure used. For such small features, however, there are a number of other factors which may limit the size. These include the effect of surface tension, the dependence of the development rate on surface curvature, and on the size of the smallest

particle that can be removed by the developer. With a pitch of 300nm, the smallest "hillocks" or "dimples" that have been fabricated have a radius of 50nm.

Reproducibility may be improved by using a larger pitch which in turn would result in larger "hillocks" or "dimples" which may be less prone to attack by the developer.

A technique of using a double exposure in a two-beam interferometer, has been shown to be able to fabricate an hexagonal array of 50-nm-radius "hillocks" or "dimples". This is made possible through the use of nonlinearities in the exposure and development processes. By using a positive resist to produce an array of "hillocks" or "dimples", the same approach may be used with a negative resist to make an array of holes. Although it is possible to fabricate such structures using electron beam lithography and laser-focused atom deposition, the technique that we have used has the potential of being a cheap and versatile alternative that avoids the need for a mask.

An embodiment of the invention has been described by way of example only, and it will be appreciated that variation may be made to the embodiment without departing from the scope of the invention. For example, the micro-cavity may be incorporated into other optical or opto-electronic devices such as an interferometer.

Claims

1. A radiation emitting device including an optical micro-cavity bounded by first and second reflective boundaries (33,39) **characterised in that** at least one of said reflective boundaries (39) has associated therewith inhibiting means to inhibit the coupling of radiation from within the micro-cavity (31) to predetermined propagation modes associated with at least one of said first and second reflective boundaries.

2. A radiation emitting device according to claim 1 **characterised in that** said inhibiting means comprises a variation in the or each refractive index of material within the microcavity.

3. A radiation emitting device according to claim 1 **characterised in that** means are provided for establishing a photonic band gap to inhibit the coupling of energy from within the micro-cavity, to modes associated with at least one reflective boundary.

4. A radiation emitting device according to claim 1 **characterised in that** the optical micro-cavity comprises first and second mirrors in which at least one of said mirrors has a substantially non-planar surface.

5. A radiation emitting device according to claim 4 **characterised in that** said nonplanar surface is in the form of a plurality of regularly spaced, undulating regions having a repeating pattern.

6. A radiation emitting device according to claim 5 **characterised in that** said nonplanar surface is arranged so that the distance, d, between said undulating regions is substantially given by,

$$2k_{spp} = 2\pi/d$$

where k_{spp} is the wave vector of a surface plasmon polariton which it is desired to inhibit.

7. A radiation emitting device according to claim 5 or claim 6 **characterised in that** said nonplanar surface is in the form of a plurality of regularly spaced, undulating regions having a repeating pattern which is generally polygonal.

8. A radiation emitting device according to claim 7 **characterised in that** said nonplanar surface is in the form of a plurality of regularly spaced, undulating regions having a repeating pattern which is generally rectangular.

9. A radiation emitting device according to claim 7 **characterised in that** said nonplanar surface is in the form of a plurality of regularly spaced, undulating regions having a repeating pattern which is generally hexagonal.

10. A method of manufacturing a radiation emitting device incorporating a sub-micron, repeating pattern in or on a dielectric substrate comprising the steps of placing a pattern bearing mask between the surface of the substrate and an energy source, exposing the substrate to the energy source and forming a pattern rotating the mask with respect to the substrate, re-exposing the surface of the substrate to the energy source thereby forming another pattern and selectively removing portions of exposed or non-exposed substrate, so as to reveal a repeating pattern on or in the substrate.

11. A method of fabricating a radiation emitting device including a substrate with a repeating pattern comprising the steps of causing a master pattern to induce a first repeating pattern to be formed on the substrate, rotating the master pattern with respect to the substrate and inducing a second repeating pattern to be formed on the substrate, the two repeating patterns sharing a common region.

12. An optical pump source **characterised in that** it includes a radiation emitting device in accordance with any one of claims 1 to 9.

13. An interferometer **characterised in that** it includes a radiation emitting device in accordance with any one of claims 1 to 9.

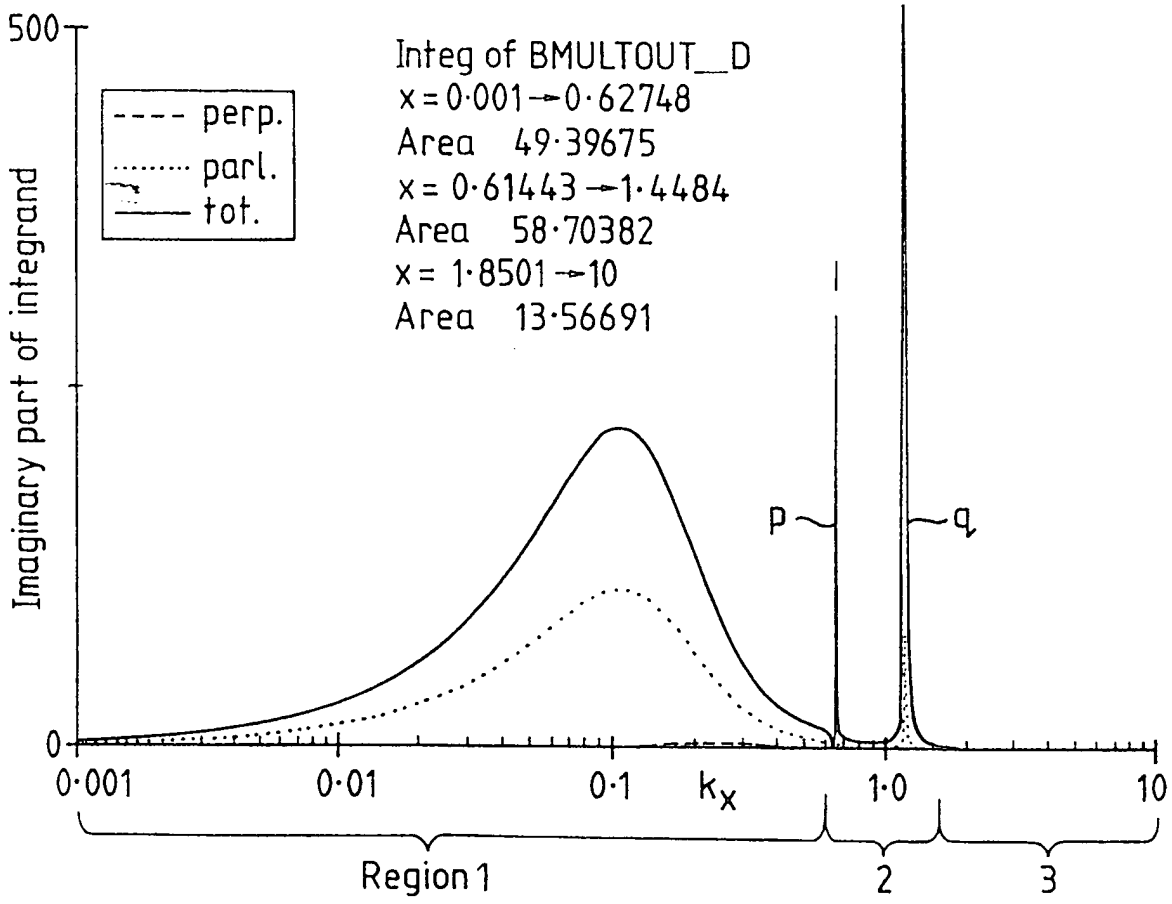
500
0
Imaginary part of integrand
---- perp.
..... parl.
—— tot.
Integ of BMULTOUT__D
x = 0·001 → 0·62748
Area 49·39675
x = 0·61443 → 1·4484
Area 58·70382
x = 1·8501 → 10
Area 13·56691
p
q
0·001
0·01
0·1
k_x
1·0
10
Region 1
2
3

Fig. 1

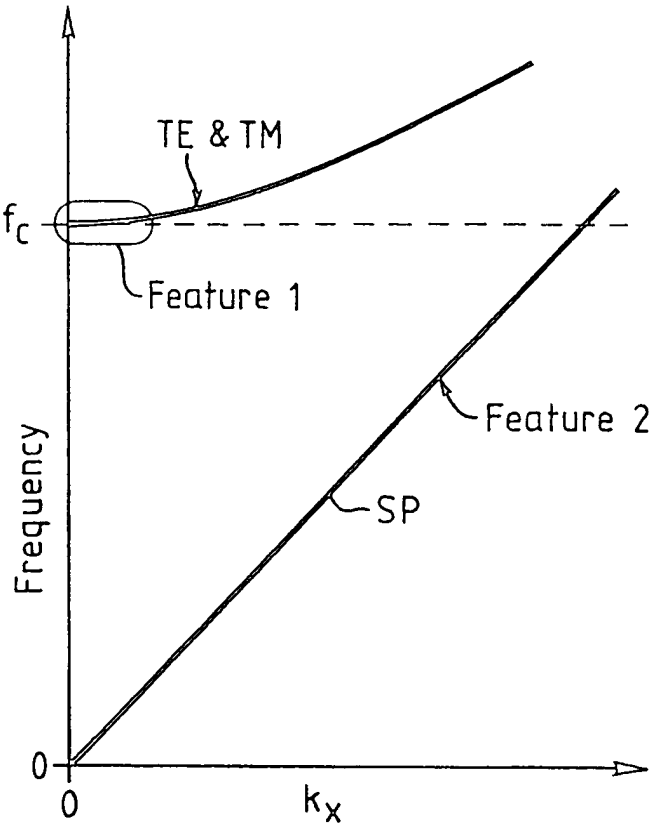
TE & TM
f_c
Feature 1
Feature 2
SP
Frequency
0
0
k_x

Fig. 2

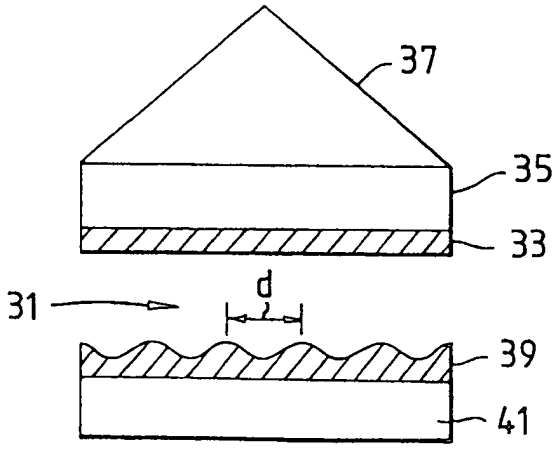
37
35
33
31
d
39
41

Fig. 3

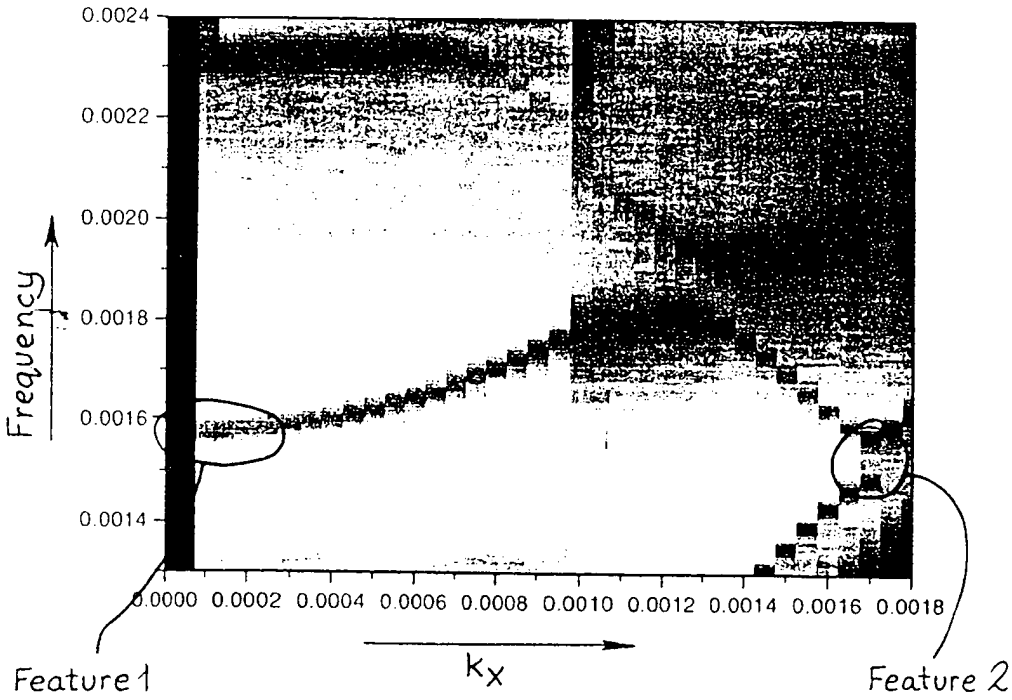
0.0024
0.0022
0.0020
0.0018
0.0016
0.0014
Frequency
0.0000 0.0002 0.0004 0.0006 0.0008 0.0010 0.0012 0.0014 0.0016 0.0018
kx
Feature 1
Feature 2

Fig. 4

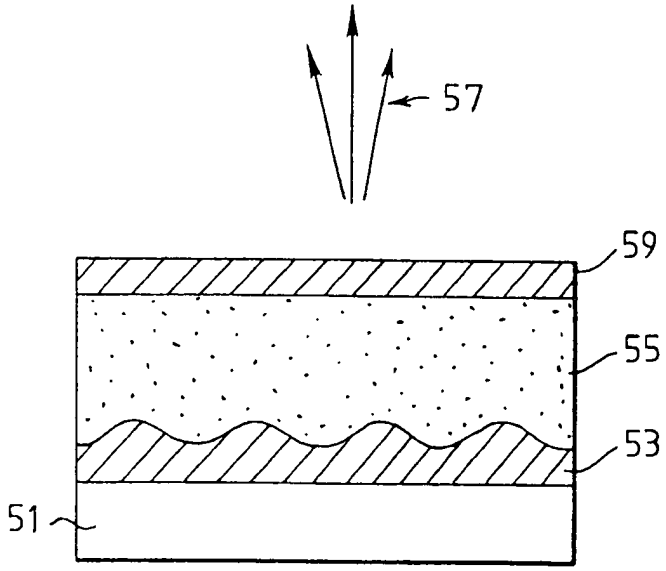
57
59
55
53
51

Fig. 5

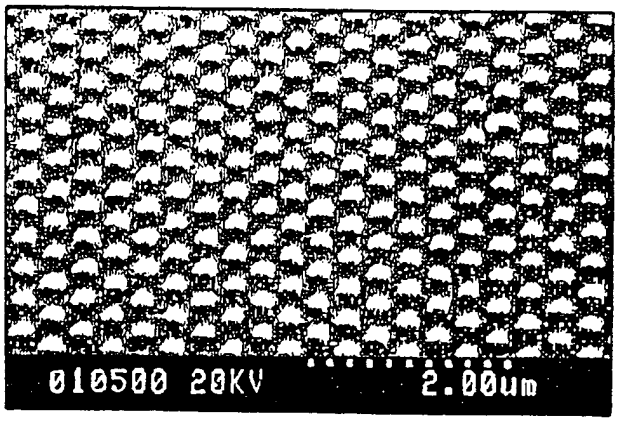

Fig. 6

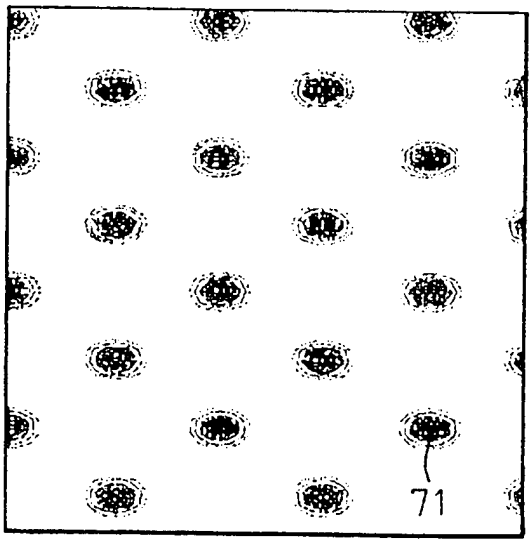

Fig 7

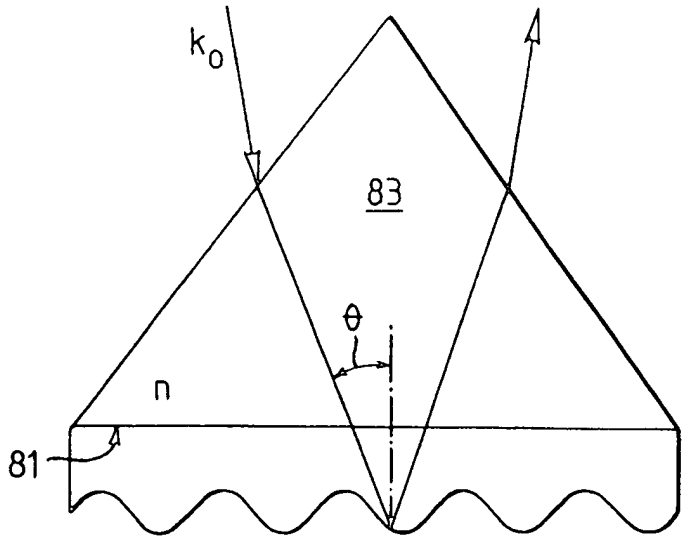
k_0
83
θ
n
81

Fig. 8

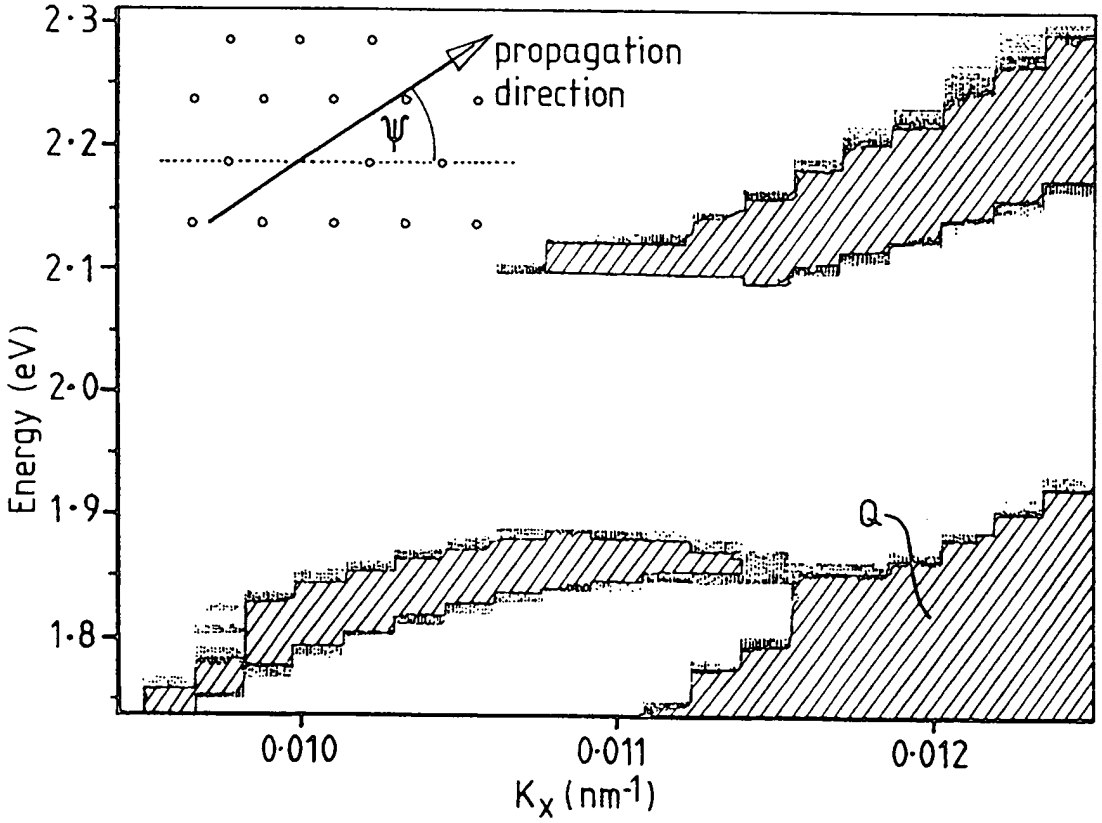
propagation
direction
ψ
Q
Energy (eV)
2·3
2·2
2·1
2·0
1·9
1·8
0·010
0·011
0·012
K_x (nm^{-1})

Fig. 9

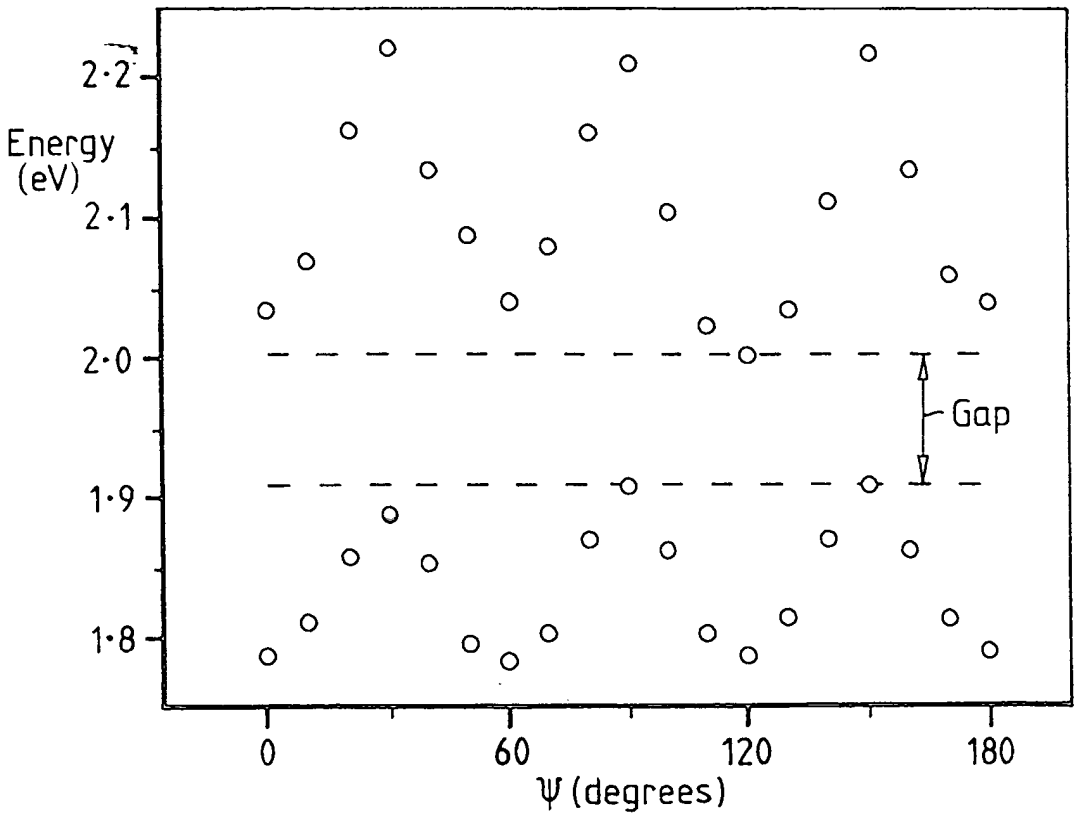

Fig. 10

INTERNATIONAL SEARCH REPORT

Interr Application No
PCT/ 97/03356

A. CLASSIFICATION OF SUBJECT MATTER
IPC 6 H01L33/00 H01S3/085

According to International Patent Classification (IPC) or to both national classification and IPC

B. FIELDS SEARCHED

Minimum documentation searched (classification system followed by classification symbols)
IPC 6 H01L H01S

Documentation searched other than minimum documentation to the extent that such documents are included in the fields searched

Electronic data base consulted during the international search (name of data base and, where practical, search terms used)

C. DOCUMENTS CONSIDERED TO BE RELEVANT

Category °	Citation of document, with indication, where appropriate, of the relevant passages	Relevant to claim No.
X	US 5 253 262 A (KUROBE ATSUSHI ET AL) 12 October 1993 see abstract; figures 11-13 see figures 20,21 see column 10, line 1 - line 46 see column 14, line 55 - column 15, line 38 ---	1-9,11, 12
A	ABRAM I ET AL: "NONGUIDING HALF-WAVE SEMICONDUCTOR MICROCAVITIES DISPLAYING THE EXCITON-PHOTON MODE SPLITTING" APPLIED PHYSICS LETTERS, vol. 65, no. 20, 14 November 1994, pages 2516-2518, XP000479890 --- -/--	1-6,12

[X] Further documents are listed in the continuation of box C.

[X] Patent family members are listed in annex.

° Special categories of cited documents :

"A" document defining the general state of the art which is not considered to be of particular relevance

"E" earlier document but published on or after the international filing date

"L" document which may throw doubts on priority claim(s) or which is cited to establish the publication date of another citation or other special reason (as specified)

"O" document referring to an oral disclosure, use, exhibition or other means

"P" document published prior to the international filing date but later than the priority date claimed

"T" later document published after the international filing date or priority date and not in conflict with the application but cited to understand the principle or theory underlying the invention

"X" document of particular relevance; the claimed invention cannot be considered novel or cannot be considered to involve an inventive step when the document is taken alone

"Y" document of particular relevance; the claimed invention cannot be considered to involve an inventive step when the document is combined with one or more other such documents, such combination being obvious to a person skilled in the art.

"&" document member of the same patent family

1

Date of the actual completion of the international search	Date of mailing of the international search report
27 February 1998	18/03/1998

Name and mailing address of the ISA	Authorized officer
European Patent Office, P.B. 5818 Patentlaan 2 NL - 2280 HV Rijswijk Tel. (+31-70) 340-2040, Tx. 31 651 epo nl, Fax: (+31-70) 340-3016	Visscher, E

INTERNATIONAL SEARCH REPORT

International Application No
T/GB 97/03356

C.(Continuation) DOCUMENTS CONSIDERED TO BE RELEVANT

Category	Citation of document, with indication, where appropriate, of the relevant passages	Relevant to claim No.
A	EP 0 698 951 A (FRANCE TELECOM) 28 February 1996 see abstract; figures 1,2 see column 3, line 43 - column 4, line 5 see column 5, line 43 - column 7, line 35 see claim 1	1-3,12
A	ABRAM I ET AL: "Spontaneous emission in planar semiconductor microcavities displaying vacuum Rabi splitting" PHYSICAL REVIEW A (ATOMIC, MOLECULAR, AND OPTICAL PHYSICS), MAY 1995, USA, vol. 51, no. 5, ISSN 1050-2947, pages 4116-4122, XP002057206 cited in the application see abstract; figures 1,5 see page 4117, column 1, line 4 - line 28 see paragraph V	1-6

INTERNATIONAL SEARCH REPORT

ormati atent family members

Intern pplication No
PCT/u. /03356

Patent document cited in search report	Publication date	Patent family member(s)	Publication date
US 5253262 A	12-10-93	JP 4273492 A	29-09-92
		JP 4167484 A	15-06-92
		DE 4135813 A	07-05-92
		US 5432812 A	11-07-95
EP 0698951 A	28-02-96	FR 2724056 A	01-03-96
		US 5701324 A	23-12-97

ELSEVIER

Synthetic Metals 101 (1999) 250–251

SYNTHETIC METALS

Effect of Lateral Microstructure on Conjugated Polymer Luminescence

B.J.Matterson[a], M.G.Salt[b], W.L.Barnes[b] and I.D.W.Samuel[a]

[a]*Department of Physics, University of Durham, South Road, Durham, DH1 3LE ,UK*
[b]*Department of Physics, University of Exeter, Stocker Road EX4 4QL,UK*

Abstract

We report a study of the effect of lateral microstructure on photoluminescence from conjugated polymers. A strong modification of the photoluminescence is observed which we assign to scattering of waveguide modes into the forward direction. This may provide a method of enhancing the efficiency of conjugated polymer light emitting diodes.

Keywords: conjugated polymers, photoluminescence

1. Introduction

There has been a lot of recent interest in the potential of luminescent conjugated polymers for use in LED displays [1]. LED structures usually proposed, consist of a thin planar layer of conjugated polymer, sandwiched between two electrodes. Indium tin oxide (ITO) is usually used as a transparent hole injecting anode and the cathode is usually a metal with a suitable work function, such as aluminium. Light generated in the polymer film through electron-hole recombination is allowed to escape through the transparent electrode.

A problem with planar LED structures is that since the layers in the device structure have a higher refractive index than the air surrounding it, the structure acts as a waveguide. A substantial fraction of emitted light is trapped in waveguide modes, rather than escaping directly through the transparent electrode. This light is not emitted in the normal viewing direction for the LED, and must therefore be regarded as a loss in overall efficiency of the device. A similar effect will also occur in photoluminescence (PL), so that most of the light generated in a polymer film may be waveguided. The higher the refractive index of the light emitting layer, the larger the fraction of light that is trapped in waveguide modes. For an isotropic material, it is easy to show [2] that only a fraction $1/2n^2$ (where n is the refractive index) of the emitted light can escape directly from the material. Conjugated polymers have a higher refractive index than most organic materials because of the polarisability associated with the delocalised π-electrons. Taking a value of two for the refractive index suggests that seven eighths of the light generated in a conjugated polymer film such as PPV could be lost to waveguide modes. A fuller treatment would require consideration of factors such as the optical anisotropy of conjugated polymer films and the roughness of interfaces.

We have investigated a new method of reducing the loss of light to waveguide modes, by breaking the planar symmetry of the luminescent films. The symmetry is broken using a corrugated substrate (resembling a diffraction grating), onto which a conjugated polymer film is deposited. The pitch of the corrugation is chosen to scatter waveguided light in the forward direction. Here we report a study of the effect of such lateral microstructure on photoluminescence from the conjugated polymer poly(2-methoxy, 5-(2'ethylhexoxy)-p-phenylene vinylene) (MEH-PPV).

2. Experimental

The grating structures were made by coating one surface of a silica slide with photoresist, and using an interference pattern to expose the surface. The interference pattern was generated by beam splitting, and recombining a laser beam. After developing the photoresist, there results a sinusoidal relief grating on the surface. The period of the grating could be altered by changing the angle between the converging laser beams at the surface. Gratings with a period of 400 nm, and a peak to trough depth of approximately 50 nm, were used as substrates for the polymer films, although it is possible to fabricate considerably shorter period gratings with this technique. Substrates with more than one grating structure superimposed can also be created with this technique. Films of MEH-PPV [3] with a thickness of approximately 160 nm were deposited on these corrugated substrates by spin coating from chlorobenzene solution (see figure 1). Planar reference films were also fabricated by following the procedure above, but without exposing the photoresist to the laser interference pattern.

Microstructured films, and planar reference films were optically excited using the 488 nm blue emission line of an

PII: S0379-6779(98)01373-3

argon ion laser, with a power of approximately 1 mW. The polymer film was kept in a cylindrical glass chamber under vacuum to prevent photo-oxidation. The resulting photoluminescence of the films was observed at various angles from the substrate using a CCD spectrometer. The light was collected and channelled to the spectormeter using a length of optical fibre, which collected only a very narrow cone of light. The apparatus was designed so that the detector could be rotated round the sample to any angle in the horizontal plane, and adjusted vertically. The excitation laser beam could also be set to any horizontal angle, within the plane of rotation. It was thus possible to observe any possible modification to the photoluminescence spectrum caused by the microstructure, at a precisely measured angle.

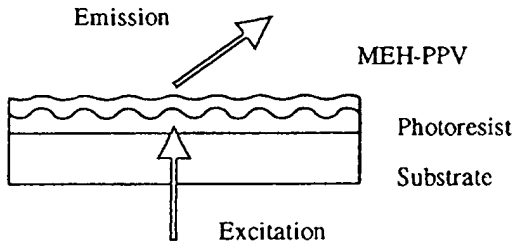

Figure 1 Experimental Geometry

3. Results and Discussion

PL spectra of MEH-PPV films on corrugated and planar photoresist coated substrates are shown in figure 2. The lower panel shows the luminescence from the MEH-PPV on planar photoresist. This shows two broad peaks at 590 nm and 630 nm and is typical of MEH-PPV photoluminescence. The upper two curves show PL spectra from a corrugated substrate. The substrate was held with its surface in the vertical plane, and the corrugation lines were aligned in the horizontal plane. For the top curve, the detector was normal to the substrate, and approximately 4 degrees higher than the excitation spot where the laser struck the polymer film. The spectrum is clearly strongly modified, now being dominated by two narrow peaks at 638 nm and 675 nm. The middle curve shows PL from the same substrate after the detector was rotated in the horizontal plane to an angle of thirty degrees from normal to the substrate. The spectral peaks are now at 625 nm and 648 nm. This demonstrates that there is a strong dependence of the PL spectrum on viewing angle.

By adjusting the detector height, it was possible to compare the dependence of PL spectra on viewing angle alterations, for detector movements perpendicular and parallel to the corrugation line direction. It was found that the peak positions were much more sensitive to the vertical detector movements (perpendicular to the corrugation lines) than the horizontal rotation. When the detector was set to be at precisely the same height as the excitation spot, the two peaks merged into a single peak. Separation of the peaks increased gradually with vertical displacement from this position. In comparison, it was found that rotating the detector away from normal angle in the horizontal plane, always caused peaks to shift to shorter wavelengths.

Figure 2 Comparison of photoluminescence spectrum of

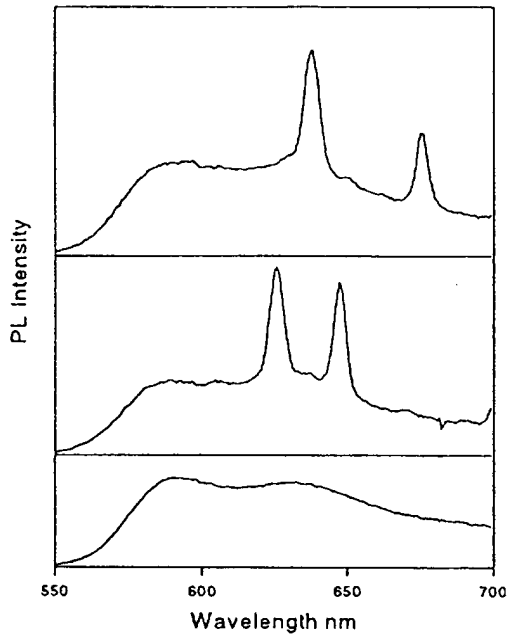

MEH-PPV on corrugated substrate (upper two curves), with flat photoresist coated substrate (lower curve).

We believe that the enhanced peaks of the PL spectra correspond to TE polarised waveguide modes that have been scattered from the polymer film. Since the MEH-PPV has a broad luminescence spectrum, the range of colours that it emits are scattered into a range of angles from the film. When the viewing angle is normal to the film, then the two waveguide modes propagating in opposite directions across the film both emit the same colour in this direction, hence the observation of a single peak.

4. Acknowledgements

We are grateful to the EPSRC Microstructured Photonic Materials Initiative and DERA Malvern for financial support. We are grateful to Hoechst for the supply of MEH-PPV. IDWS is a Royal Society University Research Fellow.

5. References

[1] D.D.C.Bradley, Current Opinion in Solid State and Materials Science 1 (1966), 789-797
[2] N.C.Greenham, Advanced Materials (1994), 6, No.6 491-494
[3] I.D.W.Samuel, Synthetic Metals 84 (1997) 497-500

High Extraction Efficiency of Spontaneous Emission from Slabs of Photonic Crystals

Shanhui Fan, Pierre R. Villeneuve, and J. D. Joannopoulos
Department of Physics, Massachusetts Institute of Technology, 77 Massachusetts Avenue, Cambridge, Massachusetts 02139

E. F. Schubert
Center for Photonics Research, Department of Electrical and Computer Engineering, Boston University, 44 Cummington Street, Boston, Massachusetts 02215

(Received 16 October 1996)

A thin slab of two-dimensional photonic crystal is shown to alter drastically the radiation pattern of spontaneous emission. More specifically, by eliminating all guided modes at the transition frequencies, spontaneous emission can be coupled entirely to free space modes, resulting in a greatly enhanced extraction efficiency. Such structures might provide a solution to the long-standing problem of poor light extraction from high refractive-index semiconductors in light-emitting diodes. [S0031-9007(97)03094-9]

PACS numbers: 42.70.Qs, 41.20.Jb

Spontaneous emission arises from the intricate interplay between a radiating system and its surrounding environment [1,2]. A prominent example of this interplay can be seen in a photonic crystal, where spontaneous emission can be enhanced, attenuated, or even suppressed by changing the density of electromagnetic states at the transition frequency [3–6], or by changing the orbital angular momentum of the emitted photon [7]. The ability to control spontaneous emission could have profound consequences on many optoelectronics devices [8].

One device that could potentially benefit from this control is the light-emitting diode (LED), which spontaneously emits radiation from a p-n junction. In the past thirty years, various approaches have been proposed to enhance the extraction efficiency of LED's [9–12]. Many of these approaches rely on clever geometrical optical designs to either enlarge the escape cone of photons using a hemispherical dome [9], or to enable multiple entry of photons into the escape cone using photon recycling [10] or surface roughness [11]. These approaches, however, do not alter directly the spontaneous emission properties of the devices. The first attempt to increase LED efficiency by direct modification of spontaneous emission was made using a Fabry-Perot type microcavity [12]. However, these resonant cavity LED's could not provide enhancement over the entire emission spectrum, but rather only when at resonance. In this Letter, we present a different approach to the modification of spontaneous emission which leads to significant enhancement over a very wide range of frequencies. Furthermore, as no resonance or photon recycling is involved, the photon lifetime is shorter, which has the effect of reducing the absorption loss and increasing the response speed. In particular, we study the effect of a two-dimensional photonic-crystal slab on the spatial distribution of spontaneous emission from a dipole moment. We show that nearly *all* the emitted light can be extracted from such a dielectric geometry.

We begin by using a simple model for the LED which consists of placing a point dipole source inside a uniform high-index dielectric slab. For concreteness, we choose a slab of thickness $0.5a$, where a is an arbitrary length unit to be defined later, and a refractive index of 3.5, typical for high-index semiconducting materials, such as GaAs, at a wavelength of 1.55 μm. The schematic diagram of the setup is shown in Fig. 1(a). The emitted radiation from the dipole source will either couple to the guided modes of the dielectric slab or to radiation modes.

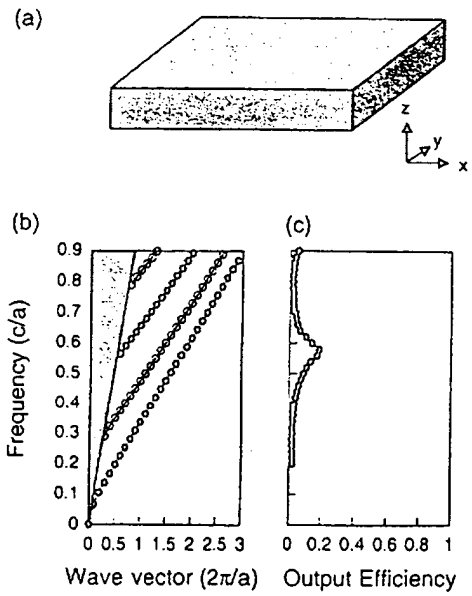

FIG. 1. (a) Schematic diagram of a uniform dielectric slab. (b) Dispersion relation of the structure shown in (a) for TE-like guided modes. The gray area corresponds to the continuum of extended (nonguided) modes. The solid circles correspond to TE guided modes with even symmetry with respect to the x-y symmetry plane, while the open circles correspond to TE guided modes with odd symmetry. (c) Output efficiency along the z direction as a function of frequency.

 0031-9007/97/78(17)/3294(4)$10.00

The dispersion relations of the guided modes are computed using a conjugate gradient plane-wave expansion method [13]. The first four TE guided mode bands are plotted in Fig. 1(b). These modes are characterized by an electric field lying within and parallel to the slab. The continuum of radiation modes is shown in gray above the light cone. We focus our attention on the TE guided modes since light emitted from a quantum well "sandwiched" between two dielectric layers would have a similar polarization. The first and third TE bands have even symmetry with respect to the mirror plane parallel to the slab [solid circles in Figs. 1(b) and 1(c)], while the other two have odd symmetry (empty circles).

We define the extraction efficiency as the fraction of emitted flux through the top and bottom surfaces of the slab to the total emitted flux. In general, we would expect the extraction efficiency to increase with the density of radiation modes, and decrease with the density of guided modes. To calculate the efficiency, we use a three-dimensional finite-difference time-domain method described in Ref. [14] with Mur's absorbing boundary conditions [15]. A point dipole source polarized in the x-y plane is inserted at the center of the dielectric slab, and is excited with a Gaussian profile in time. The extraction efficiency is shown in Fig. 1(c) as a function of frequency. The results are obtained by a discrete Fourier transform [16] which allows us to compute the efficiency at different frequencies in a single simulation run.

For the most part, the extraction efficiency is well below 10%. At low frequencies the density of radiation modes increases more rapidly than that of the single guided mode. Consequently the extraction efficiency initially increases with frequency, eventually reaching a maximum of 19% at $0.58c/a$. The drop in efficiency above $0.58c/a$ arises from the appearance of an additional guided mode which "traps" the emitted radiation and hinders light extraction from the slab. A similar drop is not observed at the cutoff frequency of the second band in Fig. 1(b) since the dipole source cannot couple to bands with odd symmetry.

The existence of guided modes in the slab impedes the extraction of light. In the case shown in Fig. 1(a) where the slab is surrounded by air, guided modes exist at every frequency [17]. By introducing a strong two-dimensional variation of the refractive index into the slab, we hope to create a frequency range for which no guided modes can exist. In this frequency range, all the spontaneously emitted power will couple to free space modes and will radiate out of the slab.

We choose to introduce an index variation by patterning a triangular lattice of air holes into the dielectric slab. The holes are chosen to have a diameter of $0.45a$, where a is the lattice constant of the triangular array. For the purpose of calculating the extraction efficiency, we choose a slab with a finite number of holes, as shown in Fig. 2(a). The triangular lattice is a natural choice since, in the case of a slab with *infinite* thickness,

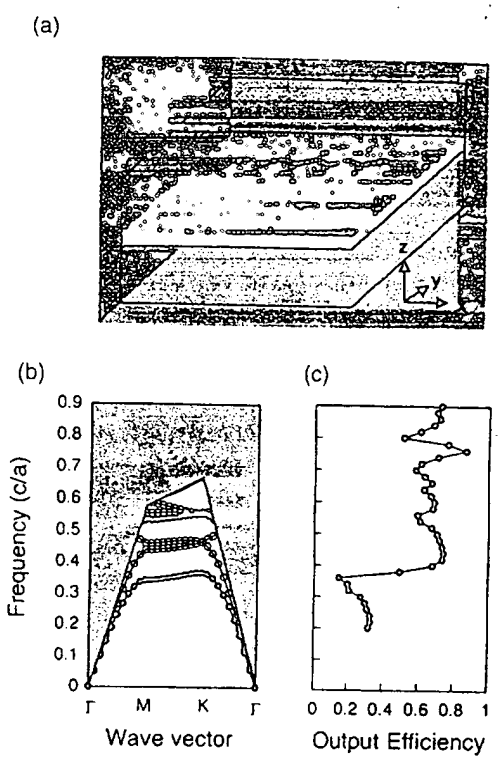

FIG. 2. (a) Schematic diagram of the computational cell containing a finite number of air holes inside a dielectric slab on a triangular lattice. (b) Dispersion relation of the structure shown in (a) for the case of an infinite number of air holes. The gray area corresponds to the continuum of extended (nonguided) modes. The solid circles correspond to TE-like guided modes, while the open circles correspond to TM-like guided modes. (c) Output efficiency as a function of frequency, for the case shown in (a).

a large in-plane band gap appears for both TE and TM polarizations [18,19].

The photonic band diagram for a corresponding slab with an infinite array of holes is plotted in Fig. 2(b). The gray region above the light line corresponds to the continuum of extended modes. Below the light line, we show the bands for every guided mode in the structure. The periodicity has a dual effect on the guided modes: it opens a gap, and also sets an upper frequency limit. A gap can be seen between the first and second TE-like bands, and between the second and third TM-like bands [20]. The first two TE-like bands are even with respect to the mirror plane parallel to the slab. The gap for the TE-like modes extends from $0.37c/a$ to $0.53c/a$ (size of 36%, which is defined as the gap width over the midgap frequency), while the gap for the TM-like modes extends from $0.47c/a$ to $0.56c/a$ (size of 17%). Above $0.66c/a$, all the modes are extended; the periodicity causes every mode above the cutoff to be Bragg scattered into the continuum.

We study the extraction efficiency for a dipole placed in the structure shown in Fig. 2(a). The dipole is located at the center of the slab, and is aligned along the y direction.

Again, only even TE-like modes will be able to couple to the emitted radiation. Results are shown in Fig. 2(c). At the band edge of the lowest band, the extraction efficiency jumps sharply from less than 15% to more than 70%. The efficiency remains close to 70% inside the entire gap region. A dip occurs around $0.55c/a$, which coincides with the upper edge of the gap. Above the second band, there are no TE-like guided modes. The efficiency oscillates around an average value of 70% with the occasional peak close to 90%.

We plot in Figs. 3(a) and 3(b) the power distribution of the electric field radiating from the dipole. The power is shown for two different frequencies, namely, $0.44c/a$ which lies inside the gap [Fig. 3(a)] and $0.76c/a$, which falls inside the continuum of extended modes [Fig. 3(b)]. In both cases, a large fraction of the power is radiated into free space, as expected.

Although both cases display large extraction efficiencies, the radiation patterns reveal important differences. In the case shown in Fig. 3(a), radiation appears to originate predominantly from the center of the array, while in Fig. 3(b) radiation appears to be more spread out. This difference is attributed to the nature of the eigenmodes in the absence of the dipole. Modes inside the gap do not propagate along the slab, thus emitted light goes directly into free space. On the other hand, modes above the light line possess large components in both the slab and free space. Emitted light, therefore, can propagate along the slab and then couple out, resulting in a more complex radiation pattern.

As we have shown in Fig. 2, light can be extracted from a dielectric slab with high efficiency using less than three periods of the triangular array in any direction around the dipole. Since only a finite number of holes is introduced into the slab, some radiation is able to escape along the slab. The radiation intensity decays away from the source, up to the edge of the array, and couples to guided modes and remains trapped inside the slab. By increasing the number of holes, one should be able to achieve even higher extraction efficiencies. One expects efficiencies approaching 100% in structures with a large number of holes.

For completeness, we also study the emission properties in an array of short dielectric posts. This configuration is analogous to the one described above, except that where there was dielectric now there is air, and vice versa. The posts have a radius of $0.15a$, a height of $0.5a$, a dielectric constant of 12.096, and are arranged on a honeycomb lattice. A schematic diagram of the structure is shown in

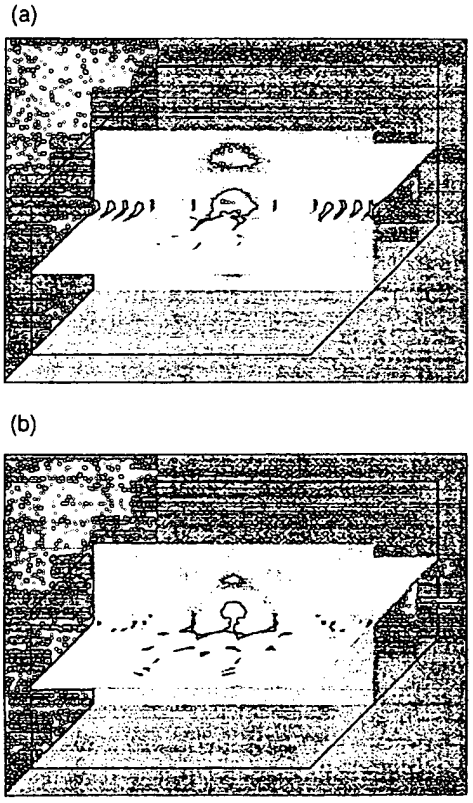

FIG. 3. Spatial distribution of the electric-field power density radiating from a dipole in the triangular lattice. The power density is shown for frequencies (a) $f = 0.44c/a$ and (b) $f = 0.76c/a$.

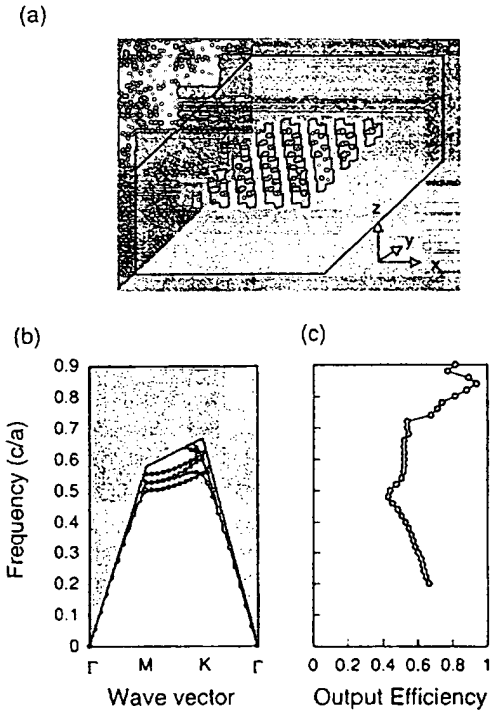

FIG. 4. (a) Schematic diagram of the computational cell containing a finite number of short dielectric posts on a honeycomb lattice. (b) Dispersion relation of the structure shown in (a) for the case of an infinite number of posts. The gray area corresponds to the continuum of extended (nonguided) modes. The solid circles correspond to TE-like guided modes, while the open circles correspond to TM-like guided modes. (c) Output efficiency as a function of frequency, for the case shown in (a).

Fig. 4(a). As was the case for the triangular lattice of air holes, the honeycomb lattice of dielectric posts generates a complete in-plane band gap for both polarizations when the posts have *infinite* length [5]. However, it turns out that the gap lies above the cutoff frequency for the guided modes (i.e., above the light line). The band structure is shown in Fig. 4(b) for the case of rods with finite length. There is no gap for the guided modes in this structure. The output efficiency is shown in Fig. 4(c). As expected, there is no spectral region with high extraction efficiency below the light cone. Above the light cone, however, the efficiency jumps above 80%, with a peak at 94%.

In conclusion, we demonstrate that efficient light extraction from a dielectric slab can be achieved with a two-dimensional photonic crystal. We present results for two different frequency regimes, namely, below and above the light cone where, in the former case, a gap is created between the guided modes. We also discuss the differences in the physical mechanisms and radiation patterns between these two regimes.

This work is supported by the MRSEC Program of the NSF under Award No. DMR-9400334.

[1] E. M. Purcell, Phys. Rev. **69**, 681 (1946).
[2] D. Kleppner, Phys. Rev. Lett. **47**, 233 (1981).
[3] E. Yablonovitch, Phys. Rev. Lett. **58**, 2059 (1987).
[4] S. John, Phys. Rev. Lett. **58**, 2486 (1987).
[5] J. D. Joannopoulos, R. D. Meade, and J. N. Winn, *Photonic Crystal* (Princeton University Press, Princeton, 1995).
[6] J. D. Joannopoulos, Brazil. J. Phys. **26**, 58 (1996).
[7] J. D. Joannopoulos, P. R. Villeneuve, and S. Fan, Solid State Commun. **102**, 165 (1997).
[8] Some examples can be found in the review article by H. Yokoyama, Science **256**, 66 (1992).
[9] W. N. Carr and G. E. Pittman, Appl. Phys. Lett. **3**, 173 (1963).
[10] I. Schnitzer, E. Yablonovitch, C. Caneau, and T. J. Gmitter, Appl. Phys. Lett. **62**, 131 (1993).
[11] I. Schnitzer, E. Yablonvitch, C. Caneau, T. J. Gmitter, and A. Scherer, Appl. Phys. Lett. **63**, 2174 (1993).
[12] E. F. Schubert, N. E. J. Hunt, M. Micovic, R. J. Malik, D. L. Sivco, A. Y. Cho, and G. J. Zydzik, Science **265**, 943 (1994).
[13] R. D. Meade, A. M. Rappe, K. D. Brommer, and J. D. Joannopoulos, Phys. Rev. B **48**, 8434 (1993).
[14] K. S. Yee, IEEE Trans. Antennas Propagat. **AP-14**, 302 (1966).
[15] G. Mur, IEEE Trans. Electromagn. Compat. **EMC-23**, 377 (1981).
[16] C. M. Furse and O. P. Gandhi, IEEE Microw. Guid. Wave Lett. **5**, 326 (1995).
[17] In the case where the slab lies on a substrate, the first guided-mode band has a nonzero cutoff frequency. The emitted radiation below the cutoff is almost entirely funneled into the substrate.
[18] R. D. Meade, K. D. Brommer, A. M. Rappe, and J. D. Joannopoulos, Appl. Phys. Lett. **61**, 495 (1992).
[19] P. R. Villeneuve and M. Piché, Phys. Rev. B **46**, 4969 (1992).
[20] TE modes are defined in a uniform slab as the modes for which the electric field is polarized parallel to the slab. In the case of a nonuniform dielectric slab, the modes are not purely TE or purely TM, but rather TE-like or TM-like.

APPLIED PHYSICS LETTERS VOLUME 74, NUMBER 16 19 APRIL 1999

Light-emitting diodes with 31 % external quantum efficiency by outcoupling of lateral waveguide modes

R. Windisch[a] and P. Heremans
IMEC, Kapeldreef 75, B-3001 Leuven, Belgium

A. Knobloch, P. Kiesel, and G. H. Döhler
Institut für Technische Physik I, Universität Erlangen–Nürnberg, D-91058 Erlangen, Germany

B. Dutta and G. Borghs
IMEC, Kapeldreef 75, B-3001 Leuven, Belgium

(Received 1 February 1999; accepted for publication 24 February 1999)

The external quantum efficiency of light-emitting diodes (LEDs) is usually limited by total internal reflection at the semiconductor–air interface. This problem can be overcome by a combination of light scattering at a textured top surface and reflection on a backside mirror. With this design, we achieve 22% external quantum efficiency. One of the main loss mechanisms in such nonresonant cavity (NRC) light-emitting diodes is coupling into an internal waveguide. Texturing the surface of this waveguide allows the partial extraction of the confined light. In this way, we demonstrate an increase in the external quantum efficiency of NRC-LEDs to 31%. © *1999 American Institute of Physics.* [S0003-6951(99)03916-9]

Light-emitting diodes (LEDs) have a wide range of possible applications ranging from illumination purposes to optical communication systems. The efficiency of LEDs has important consequences on such applications. Due to the large difference in the refractive index, the angle of total internal reflection at the semiconductor–air interface is only 16°. For conventional surface-emitting LEDs, even with internal efficiencies close to 100%, the external quantum efficiency is thus limited to values around 2%. A promising approach to overcome this problem was proposed in 1973,[1] and consists of roughening one LED surface and applying a back mirror. Light, which is internally reflected at the top surface, is scattered at the rough surface and thus changes its angle of propagation. After reflection at the back mirror, it gets a second chance to escape from the semiconductor material. A technological method to realize such a nonresonant cavity (NRC) is to make use of epitaxial lift-off and consecutive Van der Waals bonding onto a mirror in order to obtain a thin-film LED. This approach was first demonstrated by Schnitzer *et al.* in 1993.[2]

Another important issue in the design of LEDs is to avoid the generation of light underneath the top contact. In order to achieve this independently of the current level, we have implemented a current aperture fabricated by wet thermal oxidation of AlGaAs in our LEDs. Using this design, we could obtain record external efficiencies for low device currents.[3] The maximum external quantum efficiency obtained on such structures is around 20%, which is still clearly below the expected internal quantum efficiency. This is due to various kinds of loss mechanisms. One of the optical loss mechanisms is absorption, either within the LED structure itself, or in the back mirror. Another reason is the formation of lateral waveguides within the active and cladding layers of the device. In this letter, we describe the enhancement of the external quantum efficiency by the extraction of light from these waveguides.

The sample was grown by molecular beam epitaxy (MBE) on a GaAs substrate. The layer structure consists of an AlAs sacrificial layer for epitaxial lift-off, followed by an 800 nm thick *n*-doped $Al_{0.25}Ga_{0.75}As$ layer, a 120 nm thick active GaAs layer, a 130 nm thick and weakly *p*-doped $Al_{0.3}Ga_{0.7}As$ spacer layer, a 130 nm thick *p*-doped $Al_{0.98}Ga_{0.02}As$ layer for oxidation, and a 1 μm thick *p*-doped $Al_{0.25}Ga_{0.75}As$ top layer. In the first processing step a 60 μm diam device mesa is defined by wet chemical etching stopping in the spacer layer. Then, the $Al_{0.98}Ga_{0.02}As$ layer is oxidized in wet N_2 at temperatures around 380 °C for 10 min, resulting in a current aperture with a diameter between 10 and 30 μm depending on the oxidation temperature. A second wet chemical etching step down to the *n*-doped AlGaAs layer defines 60 μm diam holes for the AuGe/Ni/Au *n* contact, which are placed at a distance of 60 μm from the device mesa edge. After applying a polyimide isolation layer and lithographically opening it on the top of the device mesa, the top contact is defined such that it makes contact to the device only on top of the oxidized area and that it extends over the edge of the device mesa to form a probing pad. The polyimide is then removed from the complete surface, except under the probing pad. The LEDs processed up to this stage are used as reference devices and further referred to as "conventional LEDs." For all other device types, a back mirror is applied by epitaxial lift-off and consecutive Van der Waals bonding onto a polyimide-coated Au mirror evaporated onto a Si wafer. The resulting flat devices with a back mirror are again characterized as a reference. For the final NRC-LEDs, surface texturing is performed in addition to the application of the mirror. For surface texturing, a densely packed monolayer of randomly distributed 400 nm polystyrene spheres is formed on a water surface and transferred onto the sample.[4] In order to introduce a spacing in between the spheres, their

[a]Electronic mail: windisch@imec.be

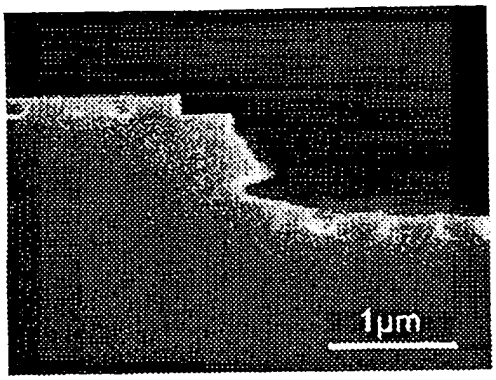

FIG. 1. Scanning electron micrograph (SEM) photograph of the textured surface on and around the mesa after removal of the spheres. The oxidized AlGaAs layer is clearly visible.

size is reduced to approximately 300 nm in oxygen plasma. This layer is used as a mask for chemically assisted ion-beam etching to an etch depth of 170 nm. Finally, the spheres are removed from the sample. Figure 1 shows the surface texturing across and around the device mesa. In contrast, a second set of NRC-LEDs is only textured on top of the device mesa, with the surface around the device being protected by photoresist during the process of surface texturing. Figure 2 shows the resulting four types of LEDs under operation.

The output power of the LEDs is measured in a calibrated[5] setup. Figure 3(a) shows the measured light output power P_{opt} as a function of the device current I for the four different types of devices. The external quantum efficiency is shown in Fig. 3(b). It is defined as

$$\eta = \frac{P_{opt}/E_{phot}}{I/q}, \tag{1}$$

with $E_{phot} = 1.42$ eV and q being the elementary charge. The conventional LEDs reach the expected external efficiency of slightly less than 2%. The application of a back mirror without surface texturing improves the light output by a factor of 5. An analysis of the local intensity distribution shown in Figs. 2(a) and 2(b) reveals that the light output within the

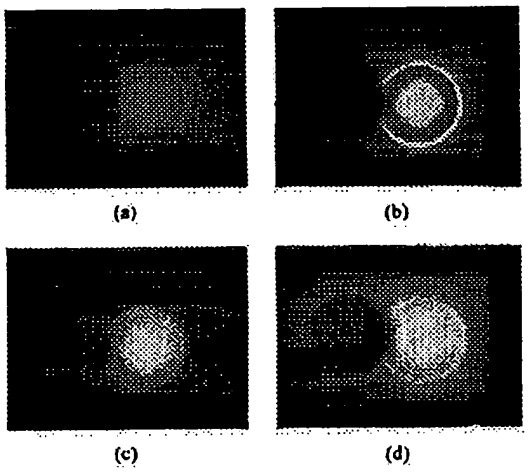

FIG. 2. CCD images of the four types of LEDs: (a) planar device without back mirror ("conventional LEDs"), (b) planar device with back mirror, (c) NRC-LED textured on top of the mesa with back mirror, and (d) NRC-LED textured everywhere with back mirror. The device currents were 45 μA for the flat devices (a) and (b) and 22 μA for the textured devices (c) and (d), respectively.

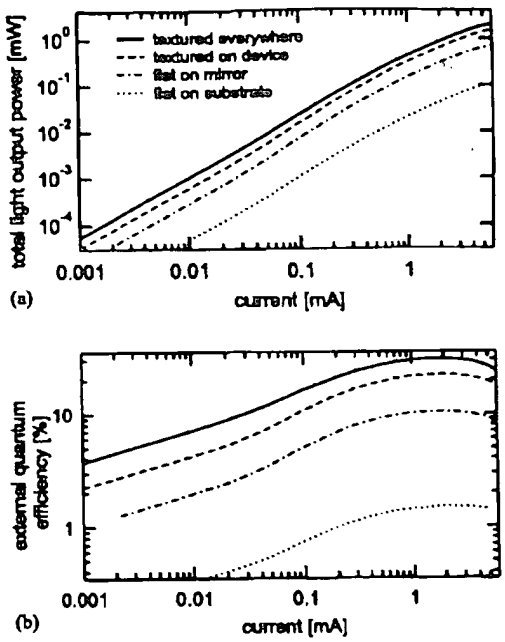

FIG. 3. Performance of the four types of LEDs: (a) log–log plot of the total light output vs injection current and (b) external quantum efficiency vs injection current.

area of the current aperture is approximately doubled, as expected from the presence of a back mirror. The remainder of the increase in the light output is due to light coupled out at the mesa edge, which is visible as a bright ring in Fig. 2(b). This is caused by the light propagating in the waveguide formed between the top surface and the oxidized AlGaAs layer. This light can be coupled out after consecutive reflections at the 55° mesa edge and the back mirror. When the top of the mesa is textured, the light is coupled out efficiently within the area of the device mesa. Such a NRC-LED, which is shown in Fig. 2(c), reaches an external quantum efficiency of 22%. By texturing not only the mesa top, but also the surface around the device, the efficiency increases to as much as 31%, as shown in Fig. 3(b). Figure 2(d) shows that this is due to the outcoupling of light from the surface around the device, which, in contrast to the LED only textured on top of the mesa [Fig. 2(c)], appears bright. Typical photon trajectories are drawn schematically in Fig. 4(c).

In order to quantify the fraction of light emitted around the device, the intensity distribution has been measured with a charge-coupled device (CCD) camera. The result is shown in Fig. 4(a). Due to the limited dynamic range of the CCD camera, the curves of Fig. 4(a) are obtained by superimposing two sets of data. The intensity distribution on top of the device mesa is measured directly. For the area around the device mesa, the same measurement is performed with a higher drive current. The symbols in Fig. 4(a) represent the intensity averaged over $10\times10\ \mu m^2$ spots measured at varying radial distances r from the device center. It is scaled to the appropriate total light output, assuming a current-independent intensity distribution. The decay of the emission in the area around the device mesa can be fitted by a function proportional to $(1/r)\times\exp(-r/r_0)$. The extension of the curves in Fig. 4(a) beyond the device edge, i.e., for $r > 30\ \mu m$, represents this fit for each of the devices. The light output for the NRC-LED textured only on top of the device

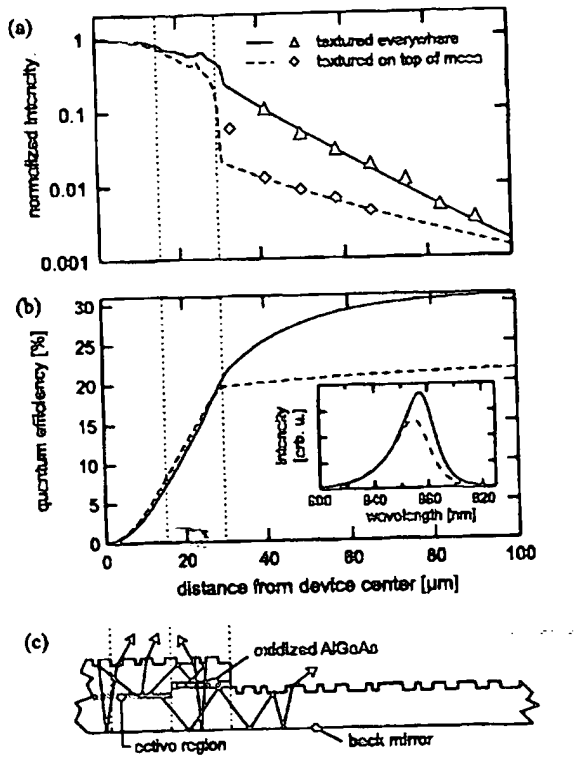

FIG. 4. (a) Intensity distribution of the two types of NRC-LEDs with mirror. (b) Integrated areal intensity as a function of the radius. The inset shows the spectrum of both device types. (c) Schematic drawing of the completely textured sample including typical photon trajectories. The scale of this drawing is identical to the axis scale in (a) and (b).

drops by more than one order of magnitude next to the mesa edge [see also Fig. 2(c)]. However, a small amount of light is also emitted from the waveguide in the flat structure around the device mesa. This is probably due to scattering at the unintended roughness introduced by wet chemical etching. If the LED is textured everywhere, a much larger amount of light is coupled out in the area surrounding the mesa. In addition to the enhancement in the external efficiency, this also leads to a faster radial decay of the emission. The decay length obtained from the fit in Fig. 4(a) for this device is $r_0 = 18\,\mu$m, in contrast to $r_0 = 45\,\mu$m for the LED only textured on top of the mesa.

The intensity emitted within a circular area of radius r can be obtained by the integration of the radial intensity distribution after multiplication by r. The result normalized to the external quantum efficiency of the respective device is shown in Fig. 4(b). It shows that within the area of the device mesa, the amount of extracted light is almost identical for both types of NRC-LEDs. As expected, the improvement of the external efficiency from 22% to 31% originates from the light emitted around the device mesa. This has a consequence for the emission spectrum. The light in the waveguide has a longer path length within the active GaAs layer. Thus, it is expected that the part of the light emitted at photon energies above the GaAs band-gap E_g is mostly reabsorbed. Recycling of the absorbed photons is unlikely, since in the area around the current aperture the carrier density is small, and thus, the radiative recombination efficiency is low. Hence, only photons with an energy below E_g can be extracted efficiently outside the device mesa. This results in an effective shift of the emission spectrum of these LEDs to longer wavelengths, as shown in the inset of Fig. 4(b).

We have presented highly efficient nonresonant cavity LEDs with a maximum external quantum efficiency of 31% obtained by the outcoupling of guided modes. We conclude that the light from guided modes can be efficiently extracted from planar waveguides by the application of a random surface texturing. This technique should also be applicable for other types of LEDs like microcavity LEDs.

The authors thank W. Van de Graaf for the MBE growth of the samples and S. Peeters for help in processing. This work was in part supported by the EC under Contract No. 22641 (OIIC). One of the authors (R.W.) acknowledges the EC for his Marie Curie Fellowship No. ERBFMICT972046.

[1] A. Bergh and H. Saul, U.S. Patent No. 3,739,217 (1973).
[2] I. Schnitzer, E. Yablonovitch, C. Caneau, T. J. Gmitter, and A. Scherer, Appl. Phys. Lett. 63, 2174 (1993).
[3] R. Windisch, P. Heremans, B. Dutta, M. Kuijk, S. Schoberth, P. Kiesel, G. H. Döhler, and G. Borghs, Electron. Lett. 34, 1153 (1998).
[4] H. W. Deckman and J. H. Dunsmuir, Appl. Phys. Lett. 41, 377 (1982).
[5] R. Windisch, P. Heremans, B. Dutta, S. Nemeth, A. Knobloch, G. H. Döhler, and G. Borghs, Proc. SPIE (in press).